Check for updates

Fibrous Scaffolds for Muscle Tissue Engineering Based on Touch-Spun Poly(Ester-Urethane) Elastomer

Juan Uribe-Gomez, Dennis Schönfeld, Andrés Posada-Murcia, Michel-Manuel Roland, Anja Caspari, Alla Synytska, Sahar Salehi, Thorsten Pretsch, and Leonid Ionov*

Development of fiber-spinning technologies and materials with proper mechanical properties is highly important for the manufacturing of aligned fibrous scaffolds mimicking structure of the muscle tissues. Here, the authors report touch spinning of a thermoplastic poly(1,4-butylene adipate)-based polyurethane elastomer, obtained via solvent-free polymerization. This polymer possesses a combination of important advantages such as 1) low elastic modulus in the range of a few MPa, 2) good recovery ratio and 3) resilience, 4) processability, 5) nontoxicity, 6) biocompatibility, and 7) biodegradability that makes it suitable for fabrication of structures mimicking extracellular matrix of muscle tissue. Touch spinning allows fast and precise deposition of highly aligned micro- and nano-fibers without use of high voltage. C2C12 myoblasts readily align along soft polymer fibers and demonstrate high viability as well as proliferation that make proposed combination of polymer and fabrication method highly suitable for engineering skeletal muscles.

1. Introduction

The development of approaches for regeneration of tissues is vitally important for future progress of medicine.[1–4] In the conventional tissue engineering approach, cells are deposited onto a supporting complex 3D structure—scaffold.[5] In order to be effective, this engineered 3D structure must be as close as possible to the native extracellular matrix (ECM).[6] ECM is formed by proteoglycans and polysaccharides, which form gel-like structures and ensure aqueous environment for cells, as well as by collagen and elastin, which form fibers and, in this way, provide suitable mechanical properties for tissues and a proper structural environment for cells. Collagen is a crystalline protein, which forms nearly nonstretchable fibers with very large elastic modulus in the order of gigapascals.[7] On the contrary, elastin is a soft amorphous cross-linked protein with elastic modulus in the order of megapascals (1–2 MPa) and could be extended to 100%, and often up to 200% before breaking.[8,9] Together, collagen and elastin ensure the J-like shape of the stress–strain curve of soft tissues, with elastic modulus in the range of tens of kilopascal at small strain and an elastic modulus of 1 MPa at 50% of extension as well as the reversibility of deformation.[8] Thus, the development of materials and methods for the fabrication of fibrous architectures mimicking the fibrous structure of ECM is highly important.

To this end, various microfabrication techniques such as photolithography,[10] melt-electro writing (MEW),[11,12] electrospinning,[13] touch spinning,[14] and their combinations have been utilized to fabricate biomimetic micro/nanoscale structures, primarily using biologically relevant materials.[15,16] For example, to the fabrication of aligned fibers, electrospinning can be used with various collectors, such as two parallel

J. Uribe-Gomez, A. Posada-Murcia, M.-M. Roland, L. Ionov
Faculty of Engineering Sciences and Bavarian Polymer Institute
University of Bayreuth
Ludwig Thoma Str. 36A, Bayreuth 95447, Germany
E-mail: leonid.ionov@uni-bayreuth.de

D. Schönfeld, T. Pretsch
Fraunhofer Institute for Applied Polymer Research IAP
Geiselbergstr. 69, Potsdam 14476, Germany

A. Caspari, A. Synytska
Leibniz-Institut für Polymerforschung Dresden e.V.
Hohe Str. 6, Dresden 01069, Germany

A. Synytska
Fakultät Mathematik und Naturwissenschaften
Technische Universität Dresden
Mommsenstrasse 4, Dresden 01064, Germany

A. Synytska
Bayerisches Polymerinstitut – BPI
Universität Bayreuth
Universitätsstraße 30, Bayreuth 95440, Germany

S. Salehi
Department of Biomaterials
University of Bayreuth
Prof.-Rüdiger-Bormann Str. 1, Bayreuth 95447, Germany

**ADVANCED
SCIENCE NEWS**

www.advancedsciencenews.com

Macro-
molecular
Bioscience

www.mbs-journal.de

bars (a relatively slow process) and a rotating drum (a faster process).[17–19] In contrast to randomly collected fibers in electrospinning, MEW technique allows deposition of uni-axially aligned fibers in a programmed way.[20–22] However, MEW is a relatively time-consuming process with an average fabrication rate of 50 mm s^{-1} and limited maximal speed of the linear actuator.[22–26] Consequently, polymers with high melting points have to be exposed to high temperatures for long periods of time in extruders, which may influence the polymer properties and structures. An alternative fiber fabrication technique introduced by Minko is touch spinning; the technique is based on touching and pulling polymer solutions or melts by a rapidly rotating rod, which draws fibers one by one upon its rotation.[27–29] The main advantages of touch spinning over MEW or electrospinning are that touch spinning allows much faster deposition of aligned fibers due to the rapid rotation of the motor and it does not require any voltage source that makes it safer for use. Recently, we showed that the aligned touch-spun fibers are promising scaffolds for muscle tissue engineering and they support the alignment of muscle cells.[14]

Common thermoplastic polymers, such as polycaprolactone (PCL) or polylactide (PLA), have a high elastic modulus in the order of hundreds of MPa (340 MPa for PCL) with a melting temperature of 60 and 160 °C, respectively. In addition, they are significantly harder than cells and tissues. On the other hand, certain polyurethane copolymers may be characterized by a lower stiffness, which makes them also interesting candidates for soft tissue engineering applications.[14,26] The yield point of polymers is, for example, affected by strain rate and temperature. Therefore, deformation conditions have to be closely considered in line with an application environment. A significant advantage of segregated polyurethane copolymers is that their thermomechanical properties can be tailored by varying the individual building blocks and the ratio of hard to soft segments. Typical strains, which may occur during deformation when stimulating the formation of muscle tissues in an engineered environment, are ≈20%.[30] When using PCL or PLA as base materials, large parts of the deformation may become irreversible at such strains, and a mechanical stimulation becomes impossible. To solve this problem, this issue was addressed here by using thermoplastic polyurethane elastomers, which can be processed in melt and solution, they can be soft and demonstrate high reversibility of deformation at large strain values.[31] According to literature, various thermoplastic polyurethanes have been used to fabricate fibers for tissue engineering applications such as polyurethane-urea,[32] poly(ester carbonate urethane)urea,[33] PCL–polyurethane,[14] and polyurethane-fibrinogen.[34]

In our previous report, several copolymers of PCL-based polyurethanes were synthesized by two-step polymerization using dimethyl sulfoxide (DMSO) as a solvent.[14] The main problem of the synthesis was applying anhydrides, due to their toxicity, and providing an inert atmosphere, which is expensive and hard to manage for industrial purposes.[35] In the current study, we report the synthesis of a poly(ester-urethane) (PEU), where we avoid the use of solvents during preparation. In this case, the reaction occurs at a higher temperature (120 °C instead of 70 °C in solution) that results in a higher molecular weight by one order of magnitude on average.

This work reports on a PEU suitable for biofabrication and capable of forming microfibers. The segmented block copolymer mainly consists of a biodegradable aliphatic polyester, poly(1,4-butylene adipate) (PBA), block-linked to each other by an aromatic polyurethane block. At body temperature, it is softer than most common polyesters ($E \approx 1$–3 MPa) in comparison with PCL ($E \approx 8$–20 MPa).[14] It demonstrates significant reversibility (above 50%) of deformation at 50% elongation, cell viability higher than 85%, and degradation in phosphate-buffered saline (PBS) around 7% per month. Obviously, the solvent-free polymerization approach opens opportunities for the production of cell and environmentally friendly materials. Therefore, our PEU could be a suitable candidate for muscle tissue engineering.

2. Results and Discussion

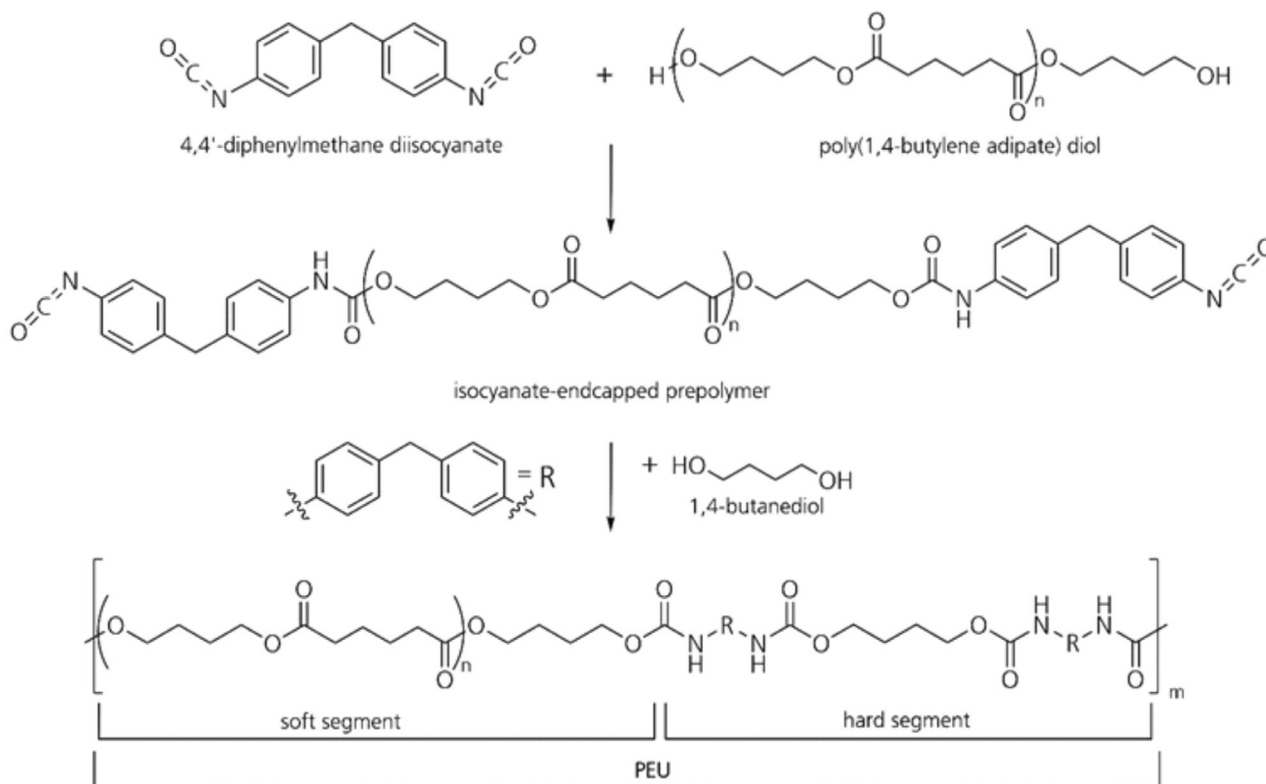### 2.1. Synthesis and Characterization

The PEU was obtained in a two-step synthesis process following the prepolymer method,[35–37] shown in **Scheme 1** and described in detail in our recently published work.[38] First, 4,4′-diphenylmethane diisocyanate (MDI) and poly(1,4-butylene adipate) diol (PBA-diol) were brought to reaction in order to build up an isocyanate-endcapped prepolymer. Afterward, the chains of the prepolymer were extended by adding BD. As a result of using building blocks with bifunctional units, a linear phase-segregated PEU block copolymer was obtained. Herein, the so-called soft segments, which impart elastic properties to the polymer in the amorphous state, were built up by PBA. In turn, the hard segments composed of MDI and BD contribute to the strength of the PEU and provide physical cross-linking to the polymer. The number average molecular weight of the TPU-PBA 25 was determined as Mn $\approx 1.4 \times 10^5$ g mol^{-1} with polydispersity indices (PDI) ≈ 2.9 (Figure S1 and Table S1, Supporting Information). The block copolymer was characterized by ^{1}H-NMR and Fourier transform infrared spectroscopy (FTIR) spectroscopy to verify the molecular structure. It is well-known from earlier works that similar polymers exhibit a high degree of reversible deformability up to several hundred percent of strain.[14,39–42]

The ^{1}H-NMR spectra show characteristic chemical shift, spin multiplicity, coupling constants, and integration of all the protons of the block copolymer (**Figure 1**a). In general, the peaks at the low field between 10.0 and 7.0 ppm were assigned to the aromatic protons and the N–H in the urethane, confirming the successful reaction. As nuclear magnetic resonance (NMR) spectra show single signals for each part of the block copolymer, it is possible to calculate the ratio between the hard and soft segment using the Equation (1),

$$HSC\% = \left(\frac{\int HS}{\int HS + \int SS} \right) \times 100 \qquad (1)$$

where HS is a hard segment, being the summary of integrals of one aromatic signal and the independent signal of BD; and SS is a soft segment from an individual signal of PBA in NMR. As a result of the calculations taking the signals at 7.07, 3.79, and 2.27 ppm, we obtained 23.9% of hard segment content, which was comparable to the composition expected (25.0%) from the ratio between the monomers used for polymerization.

**ADVANCED
SCIENCE NEWS**

www.advancedsciencenews.com

{M} acro-
molecular

Bioscience

www.mbs-journal.de

Scheme 1. Prepolymer synthesis method for the production of a phase-segregated PEU.
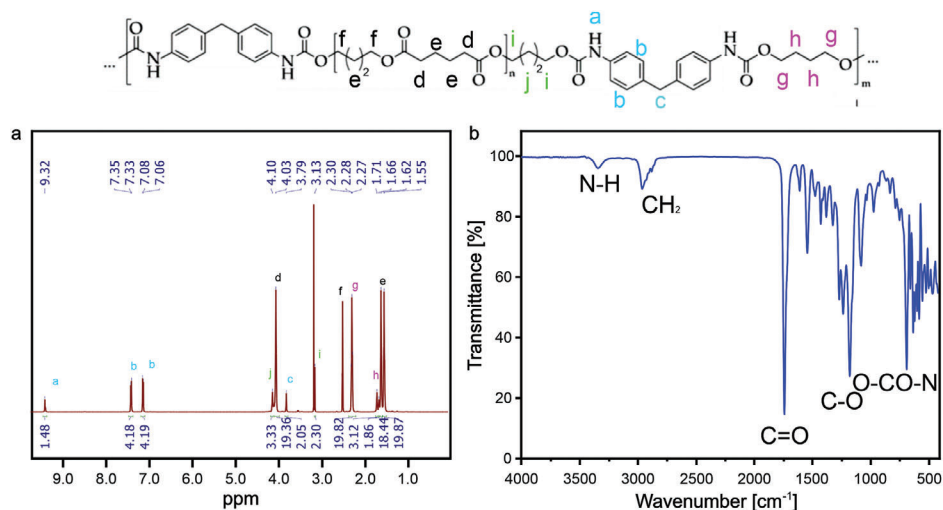

Figure 1. a) NMR spectra and b) FTIR spectra of TPU-PBA 25 block copolymer.

The FT-IR spectra (Figure 1b) shows distinct bands which are specific for the PEU. The bands at 1531 cm^{-1} and 3328 cm^{-1} correspond to the N-H bending and N–H stretching of the urethane group, respectively. The band at 1727 cm^{-1} that corresponds to the free (non-hydrogen-bonded) C=O stretching of the urethane and carbonyl groups, and the absence of a distinct signal at 2280 cm^{-1} correlated with the presence of freely available isocyanate groups are indicators of complete reaction. There is the band at 1164 cm^{-1} due to the C–O stretching of the car-

bonyl group; the bending out-of-plane of O–CO–N shows a band at 673 cm^{-1}. In the range of 3031–2796 cm^{-1} the asymmetric and symmetric C–H stretching is observed, and at 1463 cm^{-1} the asymmetric C–H bending of CH$_2$ is observed. Finally, the band located at 1596 cm^{-1} corresponds to the C–C stretching of the aromatic rings and the band at 816 cm^{-1} corresponds to the C–H bending of the p-disubstituted benzene ring. The principal FTIR signals indicate the urethane linkage in the TPU-PBA 25, which is strong indication for the synthesis of polyurethane
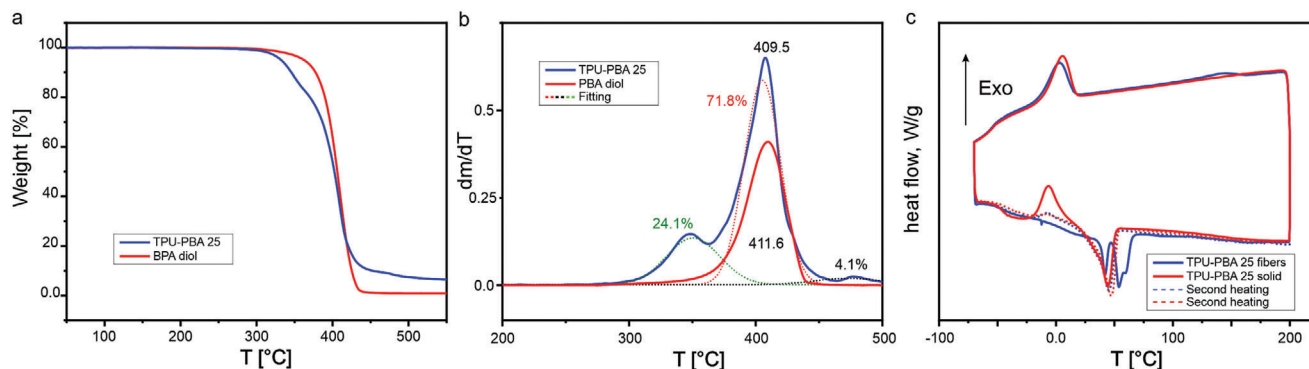
Figure 2. Thermogravimetric analysis: a) TGA from 50 to 550 °C under nitrogen atmosphere, mass loss of TPU-PBA 25, and PBA diol. b) dm/dT of TPU-PBA 25 and PBA diol. c) DSC from −70 to 200 °C at 10 °C min^{-1} of TPU-PBA 25.

Table 1. Quantitative summary of DSC data.

Polymer	T_g [°C]		T_m [°C]		ΔH [J g^{-1}]		X_c[b] [%]	
	1st heating	2nd heating	1st heating	2nd heating	1st heating	2nd heating	1st heating	2nd heating
PBA diol*	−42.0	−57.0	21	6, 30	89.3	17.5	66.14	55.0
			56	53		56.8		
TPU-PBA 25	−45.6	−42.3	−6.8[a]	−7.2[a]	15.9	0.9	28.2	19.3
			44.1	47.0	22.2	25.2		
TPU-PBA 25 fibers	−46.0	−47.5	42.1	−7.2[a]	3.6	2.6	10.7	17.7
			54.1	44.9	10.8	21.3		

* Data from Rogulska et al.[47]   [a] From cold crystallization peaks.   [b] The percentage crystallinity was calculated as: $X_c = 100\Delta Hm/\Delta Hm°$ ($\Delta Hm° = 135$ J g^{-1} for 100% crystalline PBA).[48]

copolymers.[43,44] Thus, both the results from FTIR and NMR spectroscopy confirm the successful synthesis of the TPU-PBA 25.

Thermogravimetric analysis (TGA) was performed to investigate the composition and thermal degradation of the polymer (**Figure 2**a). Pure Desmophen 2505 (PBA diol) was used as a reference sample. First, we noticed that while pure monomer demonstrates single-stepped thermal degradation with the maximum at ≈410 °C, the copolymer demonstrates clear three steps: maxima at 360, 410, and 480 °C with 24.1%, 71.8%, and 4.1% respectively, of mass loss calculated by the integration of the Gaussian fitting deconvolution (Figure 2b). The amplitude of the low-temperature decomposition step (maximum at 360 °C) in the copolymer appears corresponding to the urethane and chain extender parts (24.1% of the derivative deconvolution), meaning that the high-temperature step is attributed to the soft segment part. The composition obtained from TGA was found to be in very good agreement with the ratio between the monomers used for polymerization, 75.0% in mass of soft segment and 25.0% of the hard segment.

Thermal transitions in the PEU powder and the fibers were studied by differential scanning calorimetry (DSC) (Figure 2c and Figure S2, Supporting Information). At starting temperature of ≈−70 °C, we found that the polymer exhibits a glass transition at around −50 °C upon both heating and cooling. This is comparable to the thermal behavior of structurally related PEU.[42,45,46] Powder exhibits cold crystallization at ≈−5 °C in the first heating

cycle that was not observed in the case of fibers. Both powder and fibers have a melting peak at ≈45 °C, which is due to the melting of soft domains.[47] The fibers show a second melting peak during the first heating with a maximum at ≈50–55 °C that could be attributed to the melting of ordered domains. The fibers and powder polymer start to crystallize upon cooling at ≈5 °C. In the second heating cycle, both fibers and powder show identical behavior. The crystallinity degree of the obtained copolymer is very low: 19.3% and 17.7% in powder and fibers, respectively (**Table 1**). Thus, a similar trend was observed as recently verified for re-extruded PBA-based TPU, namely that the reprocessed polymer exhibits a slightly lower crystalline content.[46]

Meanwhile, PBA diol, which was used as a reference, showed two melting transition temperatures at 30.0 and 53.0 °C during the second heating with a total enthalpy of fusion of 74.0 J g^{-1} corresponding to a crystallinity percentage of 55.0%. The DSC of the copolymer showed a single melting endothermal signal observed between 40 and 50 °C. The introduction of PBA chains in the segmented PEU was accompanied by a restriction of chain movements, thus reducing the affinity of PBA to crystallize (Figure S3 and Table S2, Supporting Information).

2.2. Mechanical Properties

Next, the mechanical properties of the TPU-PBA 25 were characterized using dynamic mechanical analysis (DMA) (**Figure 3**a)

**ADVANCED
SCIENCE NEWS**

www.advancedsciencenews.com
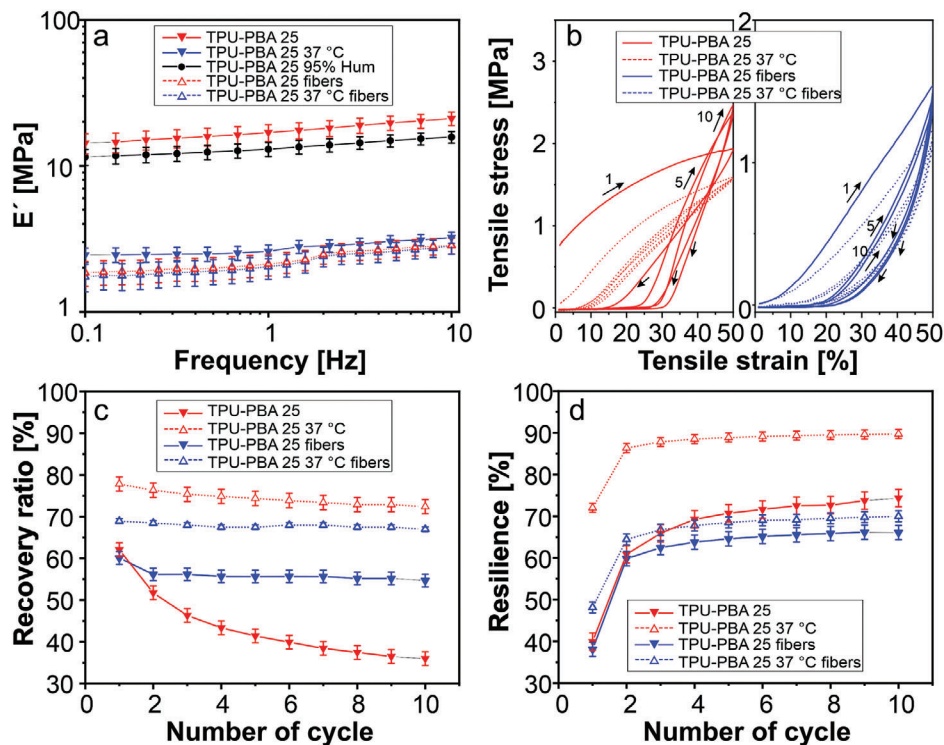
**Macro-
molecular
Bioscience**

www.mbs-journal.de

Figure 3. Mechanical properties of TPU-PBA 25. a) DMA frequency sweep, b) representative tensile test curves (cycles 1, 5, and 10 are shown), c) film and fibers recovery ratio, and d) resilience.

Table 2. Summary of mechanical properties from stress–strain cycles of TPU-PBA 25.

Polymer	E' [DMA] [MPa]	E' (cycle 1) [MPa]	E' (cycle 5) [MPa]	E' (cycle 10) [MPa]
TPU-PBA 25	17.2	14.7	12.4	11.1
TPU-PBA 25 37 °C	2.7	3.9	2.5	2.3
TPU-PBA 25 95% Hum	13.3	Was not measured		
TPU-PBA 25 fibers	2.3	1.4	1.1	0.8
TPU-PBA 25 fibers 37 °C	2.2	1.0	0.5	0.3

and cyclic tensile testing at room temperature and cell culture temperature (37 °C) (Figure 3b). It was found that the storage modulus of the copolymer in film and fibers in the measured range (from 0.1 to 10 Hz) is almost independent of frequency. Humidity at 20 °C slightly decreases the elastic modulus of the films from 17 to ≈10 MPa. An increment in the temperature from room temperature to 37 °C causes a dramatic decrease of the modulus of films from 17.2 to 2.7 MPa. Fibers are much softer than films at room temperature—elastic modulus of fiber is ≈2.3 MPa, and it almost does not change upon heating (**Table 2**). As the fibers of the copolymer are very soft, the measurement of its modulus at 95% humidity was technically impossible (Figure 3b).[49,50]

A cyclic tensile test was performed to investigate the mechanical properties in dynamic loading–unloading circumstances to evaluate the deformation reversibility of the polymer at a larger amplitude of deformation. Films and touch-spun fibers of TPU-PBA 25 were cyclically stretched to up to 50% and allowed to relax to their initial length (Figure 3b and Figure S4, Supporting Information) while recording stress. It was found that the stress–strain behavior is nearly linear in the first stretching cycle at small deformation. From the subsequent cycles in films at 20 °C, the stress–strain curves have a J-like shape showing a partial reversible deformation; when the temperature increases, this J-like shape is shifted to lower strains, increasing the recovery ratio (Figure 3c). In the case of second and further cycles from fibers at both temperatures, this J-like shape was not observed, showing an increase in the recovery ratio at 37 °C; meaning that the TPU-PBA 25 block copolymer has the ability to recover to its initial shape partially after releasing the applied force. Thus, after the first cycle, the film of the polymer partially underwent plastic and irreversible deformation, which is clear from the character of decrease of the recovery ratio in comparison to the first cycle. In the case of fibers, for which cycles were performed at 37 °C, the recovery ratio is higher and does not show any dramatic decrease, meaning that a plastic deformation is considerably lower than in the previous case. The polymer film at 37 °C can recover over 75% of its length with respect to the initial state. The recovery ratio of the fibers increases from ≈55% to 70% upon heating to 37 °C which is due to the significant softening of the polymer.

Resilience, which is a measure of a material's ability to deform reversibly without energy loss,[51] increases during the strain–stress cycling and with an increment of temperature. The resilience was evaluated for TPU-PBA 25 in films and fibers (Figure 3d). As it can be seen, all the tested samples lost the majority of the energy during the first cycle. In subsequent cycles,

**ADVANCED
SCIENCE NEWS**

www.advancedsciencenews.com

**Macromolecular
Bioscience**

www.mbs-journal.de

the energy loss decrease indicated by the resilience increase. The reason for the increment in the resilience during cycling can be explained as follows: during first stretching entanglement decoupling occurs. This may be associated with the reorientation and breaking of molecular chains, same as hardening effects associated with crystallization processes. As a matter of fact, the polymer assumes a new state of equilibrium, which does not change significantly after the second deformation.[52,53] Consequently, if the TPU-PBA 25 is used after several mechanical training cycles, we can presume constant deformation properties under cyclic loading–unloading deformation conditions.[54] It is in particular the PBA segment, which provides the elastic behavior to the PEU as long as it is in an amorphous state. Beyond reversibility of deformation after first stretching, a J-shaped stress/strain curve was witnessed. This observation is important, since it allows for mimicking mechanical properties of natural tissues.

We compared the mechanical properties of touch-spun fibers obtained in this contribution with previously reported PCL2000-HDI-BD 1:2:1 (Figure S5, Supporting Information). The main difference between PCL and PBA-based copolymers is the character of stress–strain curves obtained in the cycling stretching experiment (Figure S5a, Supporting Information). The character of recovery of stretched PCL-based copolymer is independent of temperature. In turn, PBA-based copolymer shows different ways to recover at 37 °C in both fibers and films, meaning an increment in the elastomer character of the material. During the first stretching, films and fibers of both materials at room temperature show a nonrecoverable deformation, and the recovery ratio decreases in subsequent cycles in the range of 5–20% evident in the decreasing behavior of the recovery ratio graphs during the first cycles, behavior that is not dramatic or not evidenced when the temperature increases (Figure S5b, Supporting Information). Nevertheless, fibers of PCL-based copolymer show a higher recovery ratio at 37 °C—≈85%. By contrast, fibers of PBA-based copolymer have a recovery ratio of ≈70% at the same conditions. The higher recovery ratio of the PBA-based copolymer is observed in the films at the 37 °C, and corresponds to ≈80%. The resilience of both polymers is close to each other with the exception of the fibers of TPU-PBA 25 on fibers at 37 °C that shows a resilience around 25% higher (Figure S5c, Supporting Information). This experiment clearly shows the advantage of PBA- over PCL-based copolymer, which, as we showed in the previous study, has several advantages over commonly used thermoplastic polymers such as PCL.[14]

2.3. Fiber Properties

In this study, scaffolds made by aligned fibrous were prepared by touch spinning N,N-dimethylformamide (DMF)-acetone polymer solutions. In order to optimize the touch-spinning parameters, three different concentrations were tested at three different rotational speeds at three different pressures. Uniform blob-free fibers were obtained from the three tested speeds (**Figure 4**a–c). The fiber orientation and diameter were evaluated by testing ten samples from each parameter (Figure 4d–i). It was found that the alignment of the fibers is directly affected by the pneumatic pressure applied to extrude the solutions. The increase in amplitude of the Gaussian distribution (decrease of alignment) is

directly proportional to the pressure (Figure S6, Supporting Information); the same effect was evidenced by the increment in the concentration. Speed of rotation may have twofold effect: 1) increase of the speed results in small reduction in the fiber diameter and 2) bars hit the drop forming a spray producing lower number of fibers at the high concentration of polymer. The distribution of the fiber alignment and diameter is directly affected by the bridges formed between the fibers during the processing (Figures S7 and S8, Supporting Information). After the complete analysis of the results in terms of fibers diameter and alignment, we determine that touch-spun fibers produced from the solution with low concentration (10%), high speed (1800 RPM), and low pressure (0.13 bar) show a high alignment of fibers with the smallest diameter. These fibers were chosen for further experiments and can be representative ECM for skeletal muscle tissue.

PBA is an aliphatic polyester and is a biodegradable polymer.[54] These copolymers are expected to be biodegradable, and degradation must be provided by hydrolysis of ester groups.[43,55–57] In order to prove this, we tested the real-time degradation of touch-spun fibers of TPU-PBA 25 in PBS. In this study, the hydrolytic degradation of the fibers was done by immersion in 3× PBS incubated for up to 4 weeks at 37 °C. It was found that the polymer losses about 7% in mass at week 4 (**Figure 5**b).[58] As it is revealed by scanning electron microscopy (SEM) (Figure 5a), the surface on the fibers becomes smoother after three weeks of degradation. We have also studied the change of surface charges by zeta potential of the copolymer upon its degradation (Figure 5c). For this, we performed measurements on touch spun fibers of the copolymer before and after the degradation in the PBS. The pH dependence of the fibers looks nearly similar for the fibers before and after degradation. The curves show a strong change of zeta potential in the range from pH 3 to pH 7 and plateau values with high zeta potentials around −50 mV at alkaline pH. The isoelectric point of the control sample is around pH 3.3. This is slightly acidic. For the degraded fibers, this value is shifted toward 3.8 with minor higher absolute values in the acidic plateau region. This could be an indication of a change in surface chemistry, for example, less functional groups and more hydrophobicity. This change can be explained by a decrease in the surface density of the carboxyl groups, which is due to the hydrolysis and elimination of PBA fragments[58]—it is expected that the aromatic urethane parts with linked diol shall stay nondegraded.[26] It was not observed that degraded polymer fibers change their shape upon exposure to liquid stream during zeta potential measurements (Figure 5d). Thus, these studies confirmed our expectation about biodegradability of PBA-PU block copolymer.

2.4. Cytotoxicity

Next, we have performed in vitro cytotoxicity tests based on the ISO 10993-5:2009 using two cell lines, fibroblasts and myoblasts. Indirect contact tests such as extract tests (**Figure 6**) and agar test (Figure S9, Supporting Information), allow analyzing the interaction of any leachable subproducts or dissolved polymer fragments with the cell monolayer without direct contact with the material. We observed normal morphology of both cell types after being incubated with TPU-PBA 25 fibrous scaffolds while they
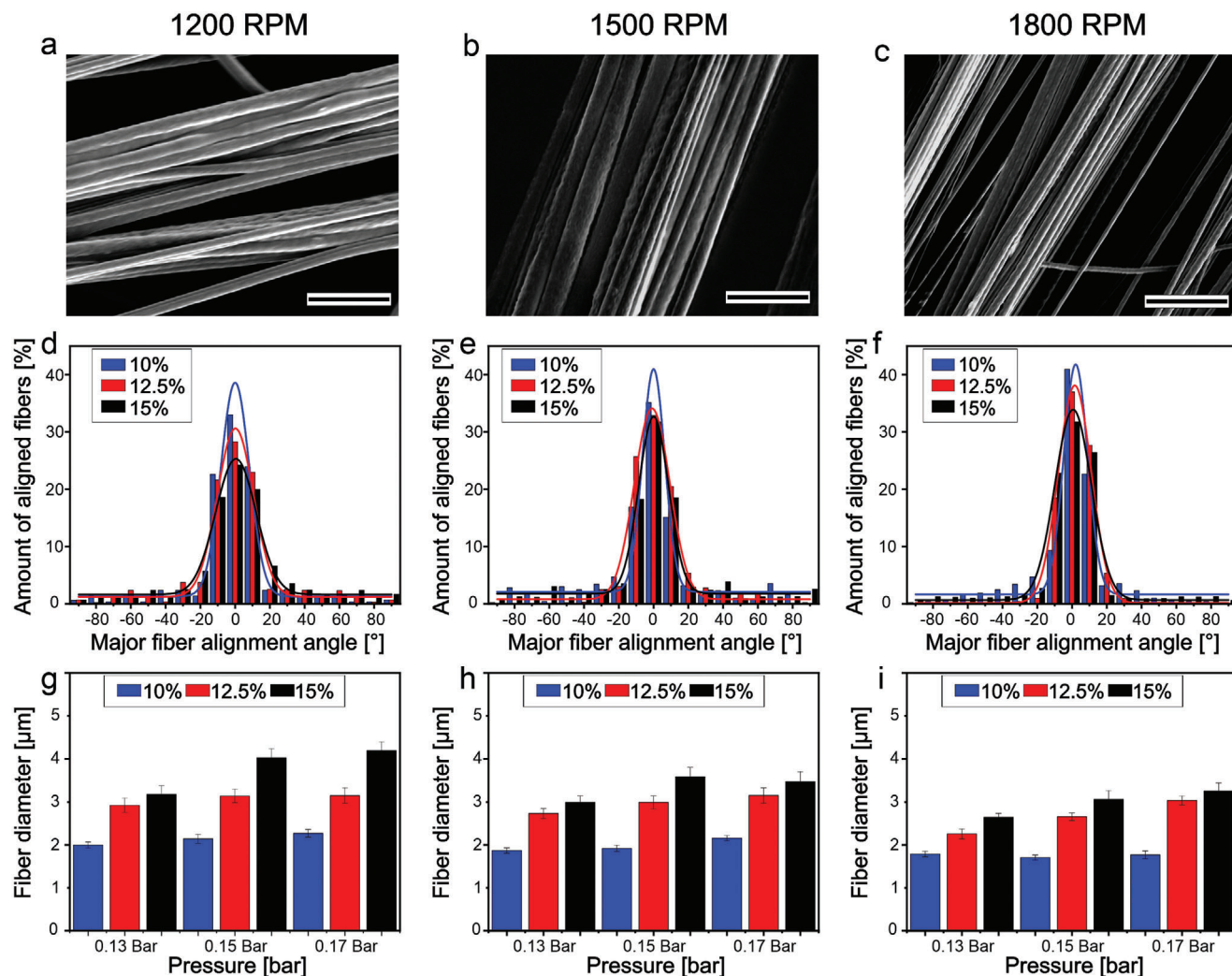
**ADVANCED
SCIENCE NEWS**

www.advancedsciencenews.com

**[M]acro-
molecular
Bioscience**

www.mbs-journal.de

Figure 4. TPU-PBA 25 fibers properties, a–c) SEM pictures of touch-spun fibers at different RPM. d–f) Major angle fiber alignment from different concentrations at 0.13 bar. g–i) Diameter of fibers from different concentrations at different pressures. Scale bars = 10 μm.

had a layer of agarose as an interface (Figure S9, Supporting Information). Their morphology had no significant difference compared to the negative control (high-density polyethylene film [HDPE]) and blank (cells cultured in a tissue culture plate without any contact with materials), while the positive control clearly caused changes in the morphology of both cell lines from adherent and spread cells to the round shape and detached cells. Cells exposed to the zinc-diethyldithiocarbamate (ZDEC), the positive control, were less spread compared to the cells in the negative and blank control. Moreover, most of the cells were detached, a sign of necrotic cells. Thus, the polymer is biocompatible.

Further, cells after 24 h contact with the extract of materials and controls were analyzed by using Alamar blue, live/dead staining, and fluorescent imaging. These tests also showed intact and normal cell morphology after being exposed to the extracts of the TPU-PBA 25 fibrous scaffolds, negative, and blank control; while, cells in contact with the extract of positive control (ZDEC) did not survive, and no image could be taken from the dead cells as they were washed away during the staining. Quantitative analy-

sis of CellTiter-Blue assay and live/dead assay (Figure 6d,h) confirmed high viability percentage of cells (nearly 100%) for TPU-PBA 25 fibrous scaffolds.

2.5. Cell Proliferation and Alignment

Finally, we performed cell culture studies on the TPU-PBA 25 fibrous scaffold with a fiber diameter 1.7 μm and 81.0% of alignment. For this, proliferation, cell viability, and nuclei alignment were quantified on scaffold with initial cell density of 150.000 cells cm^{-2}. The results showed that after 7 days of culture, only a few cells adhered to the fibers. In order to improve and compare cell adhesion, the scaffolds were treated with FNC (fibronectin mixture). The metabolic activity and viability of the cells were studied on coated, noncoated scaffolds and treated cell culture plates (Figure S10, Supporting Information). It is clear from the results that the cell's metabolic activity and viability are high in the cell culture plates and increase with time. On the
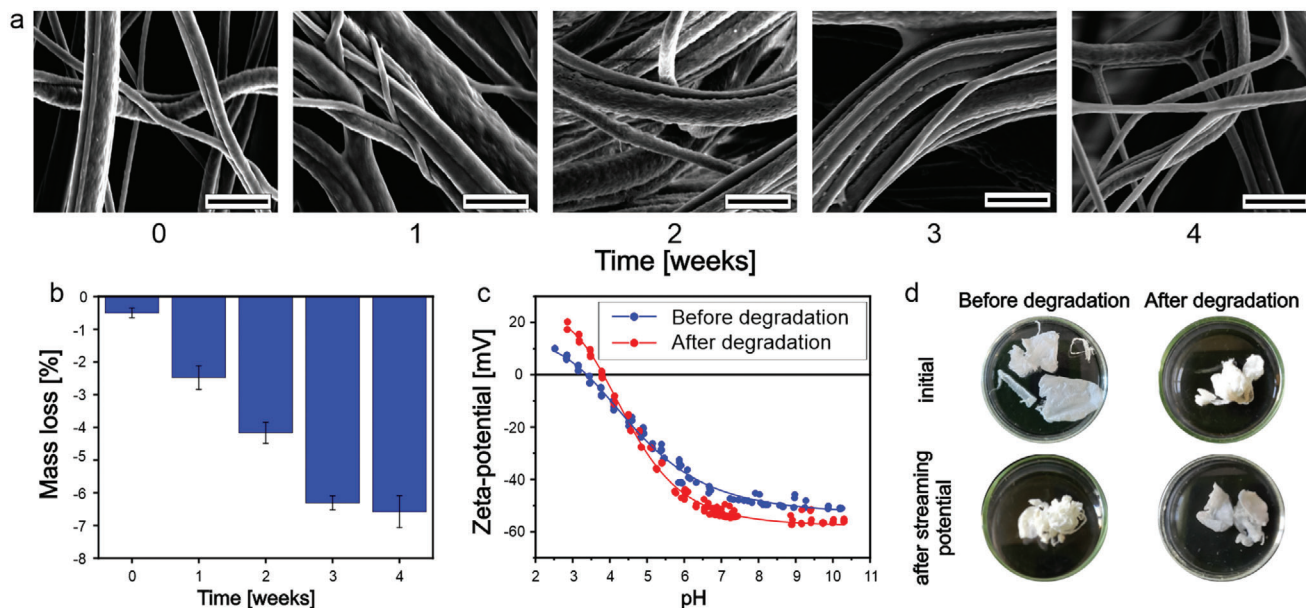
Figure 5. Degradation test of TPU-PBA 25: a) Morphology of touch spun fibers after 0, 1, 2, 3, and 4 weeks immersed in PBS solution at 37 °C. b) Mass loss of touch spun fibers during 4 weeks of degradation. c) Zeta potential of TPU-PBA 25 fibers before and after degradation test. d) Images of fiber bundles before and after degradation test and, before and after exposure to a liquid stream of zeta potential measurements. Scale bars = 10 μm
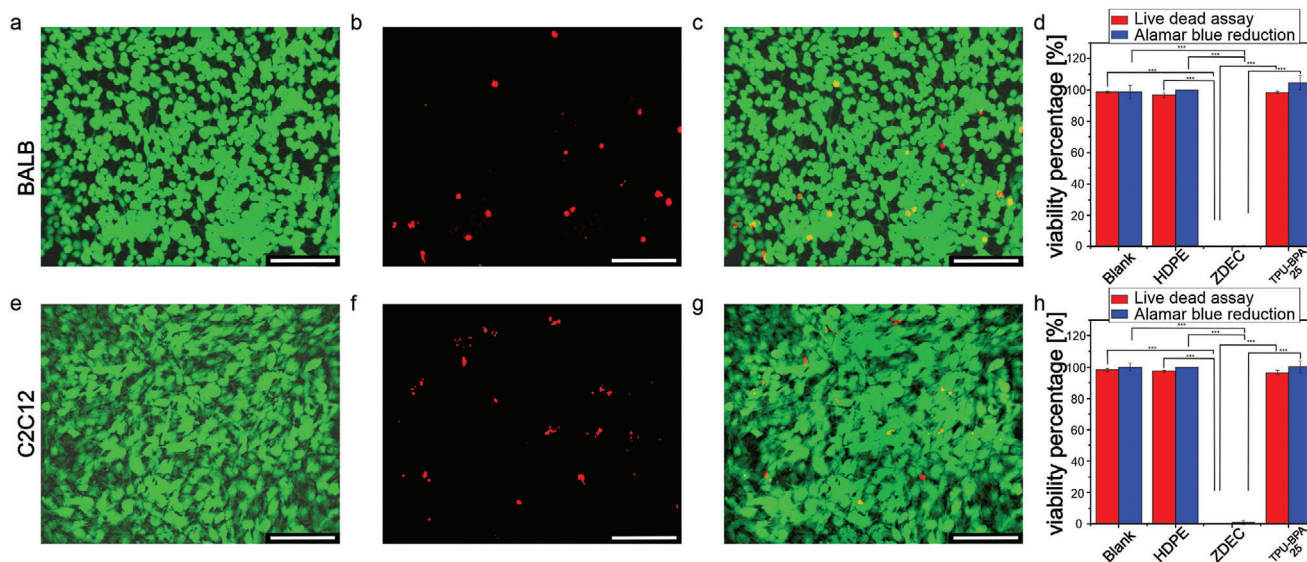

Figure 6. Qualitative and quantitative analysis of the cytotoxicity of the TPU-PBA 25 fibrous scaffold on fibroblasts and muscle cells. a–c) Fluorescent images of fibroblasts and e–g) myoblasts, taken after 24 h exposure to extract of TPU-PBA 25 fibrous scaffolds. Live/dead assay shows green (live) cells stained with calcein AM, and red (dead) cells stained with ethidium homodimer. Quantitative measurement of cell viability using CellTiter-Blue cell viability assay and live/dead assay for d) fibroblasts and h) myoblasts. Blank (cells with no contact to materials), HDPE (negative control), and ZDEC (positive control). Data are presented as the mean ± standard deviation; ***p value ≤ 0.001. Scale bar = 150 μm.

other hand, the nontreated scaffolds present the lowest metabolic activity and viability but are not significantly different from the coated ones. The major difference between the scaffolds is the number of cells attached to the surface, being higher on the scaffolds coated with FNC. Moreover, seeded cells distributed and adhered uniformly on the top of the fibrous scaffold (**Figure 7**a–d). Additionally, cells begin to align along and on the top the fibers. Interestingly, in concordance with our previous work,[14] it was found that cells proliferate and reaches 86% of viability after 7 days in culture that is lower than that measured in our previous PCL-based polyurethanes fibers produced by touch spinning[14] but higher than our previous studies on scaffolds produced by melt electrowriting.[26] Cell proliferation is also faster on the coated scaffolds than noncoated ones (Figure 7e).
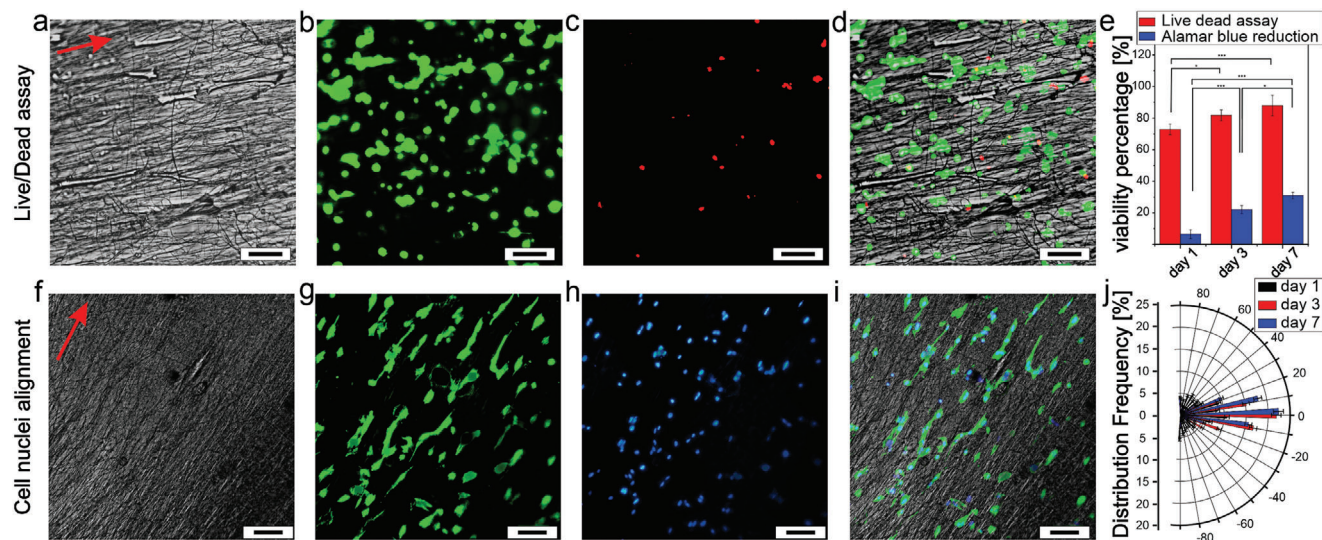
**ADVANCED
SCIENCE NEWS**

www.advancedsciencenews.com

[M]acro-
molecular
Bioscience

www.mbs-journal.de

Figure 7. C2C12 myoblasts cell culture. a–d) Live/Dead assay on TPU-PBA fiber scaffolds. Green—live cells and red—dead cells; at day 7 of culture. e) Quantification of cell viability and cell metabolic activity after 1, 3, and 7 days of culture measured by Alamar Blue assay. f–i) Cell nuclei alignment on TPU-PBA fiber scaffolds at day 7 of culture. j) Quantification analysis of cell nuclei alignment. $*p \leq 0.05$; $**p \leq 0.01$; $***p \leq 0.001$. Scale bars = 100 μm.

Cell alignment on TPU-PBA 25 fiber scaffold, coated and noncoated with FNC, was quantified after staining cell nuclei and the actin filament. Staining experiments verified the tendency of the cells to grow in the direction of the fibers and on top of the scaffold (Figure 7f–I and Figure S11, Supporting Information). It was found that the nuclei cell alignment increases with time during cell incubation: on day 1 ≈25% of cells are aligned, on day 4 ≈50% of cells are aligned, and after 7 days in culture ≈56% of cells are aligned, showing statistically significant ($p \leq 0.001$) between all the time points for the cells cultured on coated scaffolds. On the other hand, the noncoated scaffolds show similar results in terms of percentage of alignment, 25%, 40%, and 51% for days 1, 4, and 7, respectively. Even though there are no major differences between the alignment on the coated and noncoated scaffolds, the number of cells attached to the scaffolds coated with FNC is three times higher than that on noncoated scaffolds. It must be noted that if the angle formed by the cells with the main orientation of the fibers was in the range of −10° and 10°, the cells were considered aligned. Notably, cell alignment is not that high as the alignment of fibers (Figure 7j). This deviation can be explained by distance between fibers allowing the cells to form bridges in the gaps between the fibers them and change the orientation. The cell alignment improved after 7 days of culture due to the fact that cells prefer to grow following the directionality of the fibers and in the spaces in between them, instead of forming bridges between two or more fibers (Figure 7j). Also, they prefer to elongate along the fibers to form connections with other cells.

3. Conclusion

In this work, we report an approach for the fabrication of highly aligned microfibrous scaffold. Therefore, a new thermoplastic polyurethane elastomer with soft segments made from PBA was synthesized and touch spinning technique was used to prove the suitability of the copolymer for muscle tissue engineering. In this regard, a promising combination of mechanical and

thermal properties could be verified at human body temperature as evidenced by highly reliable elastomeric properties after the first loading–unloading cycle. The reported polymer demonstrates superior mechanical properties compared with PCL-based polyurethanes previously reported, and is characterized by an excellent biocompatibility that enables its use for fabrication of fibrous scaffolds allowing high cell alignment required for regeneration of such anisotropic tissues as muscle tissue.

4. Experimental Section

Materials: MDI (Fisher Scientific), 1,4-butanediol (BD, Alfa Aesar), molecular sieves (pore size of 4 Å, Alfa Aesar), Desmophen 2505 (hydroxyl-terminated PBA-diol [$Mn = 4000$ g mol^{-1}, Covestro Deutschland AG]), DMSO (Sigma-Aldrich), DMF (Sigma-Aldrich), acetone (Sigma-Aldrich), ethylenediaminetetraacetic acid (EDTA, Sigma-Aldrich), calcium chloride dehydrate (Sigma-Aldrich), Dulbecco's phosphate buffered saline (DPBS, Sigma-Aldrich), Dulbecco's Modified Eagle Medium (DMEM, Merk), penicillin–streptomycin (Pen/Strep, Gibco), gentamycin sulfate (Sigma-Aldrich), fetal bovine serum (FBS, Merck), FBS Gold Plus (Serena), GlutaMAX (Gibco), 4-(2-hydroxyethyl)-1-piperazineethanesulfonic acid) (HEPES, Carl Roth), Trypsin/EDTA (0.05%, Sigma-Aldrich), Trypan-Blue reagent 0.4% (Sigma-Aldrich), calcein-AM (Thermo Fisher Scientific), ethidium EthD-1 (Thermo Fisher Scientific), phalloidin DyLight 488 (Thermo Fisher Scientific), 4′,6-diamidino-2-phenylindole (DAPI, Thermo Fisher Scientific), Alamar Blue HS Cell Viability Reagent (live/dead assay) (Thermo Fisher Scientific), FNC solution (fibronectin, collagen, albumin mixture, Athena Enzyme Systems), and triton X-100 (Sigma-Aldrich) were used as received. The C2C12 myoblast (passage number less than 7) was purchased from ATCC (Manassas, VA). M-MSV-BALB/3T3 fibroblasts were purchased from the European Collection of Authenticated Cell Cultures (Public Health England). Agarose NEEO ultra quality was purchased from Roth. HDPE (Hatano Research Institute) and polyurethane film containing ZDEC (Hatano Research Institute) were used as negative and positive controls in ISO Standard tests 10993-5.

Synthesis of TPU-PBA 25: The prepolymer method was applied to synthesize a PBA-based PEU (Scheme 1). Therefore, 0.037 mol of PBA-diol was melted and dried in a vacuum oven at 80 °C overnight. At the beginning of the synthesis, the PBA-diol was heated to 120 °C under nitrogen flow and stirring. Afterward, 0.157 mol of molten MDI was added. After

**ADVANCED
SCIENCE NEWS**

www.advancedsciencenews.com

Macro-
molecular
Bioscience

www.mbs-journal.de

90 min of continuous stirring, the isocyanate-endcapped prepolymer was converted to PEU by adding 0.120 mol of BD. At the same time, the stirring speed was increased, and changes in viscosity were followed with an IKA Eurostar 60 control from IKA-Werke GmbH & Co. KG (Staufen, Germany). As soon as the melt viscosity increased significantly, corresponding to a rise in torque by a factor of five, the polymer melt was poured onto a plate, which was covered with polytetrafluoroethylene. Finally, the obtained PEU was cured for 120 min in a convection oven at 80 °C, before it was ground to granules.

Nuclear Magnetic Resonance Spectroscopy: The NMR spectra of TPU-PBA 25 were obtained using a Bruker Avance 500 spectrometer (Bruker BioSpin GmbH, Silberstreifen, Germany) (500.16 MHz for ^{1}H). ^{1}H NMR chemical shifts (δ) were reported in parts per million (ppm) relative to tetramethyl silane, with the residual solvent peak used as an internal reference using DMSO-d$_6$. 500 MHz, DMSO-d$_6$, δ = 9.32 (s, 2H), 7.34 (d, J = 8.0 Hz, 6H), 7.07 (d, J = 8.4 Hz, 6H), 4.10 (s, 4H), 4.03 (s, 26H), 3.79 (s, 3H), 3.13 (s, 3H), 2.28 (s, 28H), 1.71 (s, 4H), 1.66 (s, 3H), 1.62 (s, 26H), 1.55 (s, 28H).

Fourier Transform Infrared Spectroscopy: FTIR spectra were measured in transmittance mode using a Bruker Tensor 27 (USA) spectrometer with spectral data spacing of 4 cm^{-1} from 400 to 4000 cm^{-1}. The main bands in these spectra were stretching vibrations of NH groups in the 3500 to 3000 cm^{-1} range; the symmetric and asymmetric stretching vibrations of −CH$_2$ groups (v = 2950 and 2820 cm^{-1}). The characteristic stretching vibration of carbonyl group C=O (v = 1728 cm^{-1}) and C−N stretching (v = 1531 cm^{-1}) confirmed the presence of urethane groups; also, the absence of distinct signal at 2280 cm^{-1} associated with the presence of freely available isocyanate. The stretching vibration of the C−O−C bond (v = 1596 cm^{-1}) and the stretching bands from the C−O bond of the ester group (v = 1220 and 1165 cm^{-1}) corresponded to the PBA part of the copolymer.

Gel Permeation Chromatography: Gel permeation chromatography was used to determine the molecular weight (number average molecular weight [Mn], weight average molecular weight [Mw] and PDI using an instrument with 2 PSS-GRAM gel columns (particle size = 10 µm) with porosity range from 100 to 3000 Å (PSS, Mainz, Germany) together with a refractive index detector (Agilent Technologies). DMF (HPLC grade) with lithium bromide (5 g L^{-1}) was used as a solvent (for dissolving polymer and as eluting solvent) with a flow rate of 0.5 mL min^{-1}, toluene (HPLC grade) was used as an internal standard. The calibration was done with narrowly distributed polystyrene (homopolymers, PSS calibration kit). An injection volume of 100 µL was used for all the measurements. The samples were dissolved in DMF and filtered through a 0.22 µm PTFE filter before analysis.

Differential Scanning Calorimetry: The thermal behavior of the copolymer was investigated using DSC (DSC3, Mettler Toledo, USA). DSC measurements were performed by loading 5–7 mg of the polymers in a closed aluminum crucible. Three different scans were performed. In the first one, the sample was scanned in three steps: 1) heating from −70 to 200 °C to eliminate any thermal history, keeping at 200 °C for 5 min, 2) cooling down to −70 °C and keeping at −70 °C for 5 min, 3) heating to 200 °C with temperature rates of 10 °C min^{-1}. The second one: 1) heating from −70 to 70 °C and keeping at 70 °C for 5 min, 2) cooling down to −70 °C, keeping at −70 °C for 5 min, and 3) heating to 70 °C with a temperature rate of 10 °C min^{-1}. The third one: 1) heating from 20 to 200 °C and keeping at 200 °C for 10 min, 2) cooling down to 20 °C, keeping at 20 °C for 10 min, and 3) heating to 200 °C again with a temperature rate of 1 °C min^{-1}.

Thermogravimetric Analysis and Degradation Test: TGA (TGA 2 STAR System, Mettler Toledo [USA]) was performed from 30 to 550 °C at a heating rate of 10 °C min^{-1} under a nitrogen atmosphere. A real-time degradation test of the TPU-PBA 25 fibers was also performed by testing at various time points such as 1, 2, 3, and 4 weeks in PBS solution at 37 °C. PBS was changed every 3 days to ensure a constant pH during all degradation. Samples were weighted after freeze-drying and characterized by SEM at each time point. Three samples of each time point were tested.

Mechanical Testing: Thin-film of TPU-PBA 25 was cast on a glass slide from 25 wt% solutions in DMF at room temperature. After the film was air-dried at room temperature for 48 h, it was manually removed and placed

into a vacuum desiccator for 3 days to ensure complete evaporation of the solvent. Rectangular strips ($\approx$10 × 4 × 0.4 mm) and fiber scaffolds ($\approx$10 × 2 × 0.1 mm) were prepared for mechanical tests. Tensile tests were performed on a DMA (MCR 702 MultiDrive Anton Paar, Austria) equipped with Solid Rectangular Fixtures (SRF5) and a temperature chamber (CTD 600 TDR). During the measurement, static (120 kPa) and dynamic forces (120 kPa) were applied, within a frequency range from 10 to 0.1 Hz, to characterize the elastic properties of the material in extension-deformation mode. The measurements were performed at 20 and 37 °C for fibers and films, separately; the films alone were measured in a humidity controller chamber at 5% and 95% relative humidity.

Cyclic tensile tests of films and fibers were performed using the same configuration of DMA to investigate the sustainability of the copolymer. The samples were loaded and prestretched until a force lecture around 0 N was achieved, then stretched at 1% min^{-1} to 50% strain and released at 1% min^{-1} until initial length for 10 consecutive cycles; the samples were tested at 20 and 37 °C. From the recorded tensile strain–stress data, the percentage recovery ratio (R_r) of each cycle was calculated using Equation (2),

$$\%R_r = \left(1 - \frac{\epsilon}{\epsilon_0}\right) \times 100 \qquad (2)$$

where ϵ was the residual strain after the unloading steps and ϵ_0 was stretching amplitude, which in the authors' case was 0.5 (50%). The property of materials to absorb energy after elastic deformation was named resilience (R_e) and was calculated using Equation (3),[43]

$$\%R_e = \left(\frac{W_{unload}}{W_{load}}\right) \times 100 \qquad (3)$$

where W_{unload} represented the area under the stress–strain curve in the release step, and W_{load} represented the area under the stress–strain curve in the stretch step.

Touch Spinning: Touch spinning was performed in a custom-made touch-spinning device similar to one published by Minko.[27] The TPU-PBA 25 was dissolved in DMF at room temperature under magnetic stirring for 6 h, and then acetone was added to obtain a ratio of 2:1 DMF:acetone (acetone must be added to enhance the solvent evaporation during processing). The solution concentrations were optimized to yield continuous bead-free fibers with the smallest possible diameters. The final concentrations were 10%, 12.5%, and 15% w/v. The prepared solutions were loaded into a plastic dispenser with an 18-gauge PTFE blunt-end needle (I.D. 0.838 mm). Touch spinning was performed with a rotating rod attached to a wheel/disc and stable-bridged collector, distances of 1.0 mm and 5.0 cm correspondingly; the separation between the parallel bars in the collector was 2.5 cm. Rotational speed applied was 1250, 1500, and 1800 rpm, and feeding air pressure was 0.13, 0.15, and 0.17 bars.

Streaming Potential Measurements: Zeta potential was determined with SurPASS 3 (Anton Paar, Graz, A) by streaming potential measurements. 50 mg of the fibers were fixed with membranes, pore size 20 µm, in the powder sample holder. This part was inserted in the cylindrical cell equipped with Ag/AgCl electrodes. The permeability index was adjusted to around 100. The electrolyte solution was KCl, C = 10–3 mol L^{-1}. The pressure was changed in the range from 600 to 200 mbar. The measurements were initiated at neutral pH. For pH-adjustment solutions, HCl or KOH (C = 0.1 mol L^{-1}) were used. Fibers before and after real-time degradation were tested.

Scanning Electron Microscopy: SEM (Apreo, Thermo Fisher Scientific, USA) was used to characterize the morphological properties of TPU-PBA 25 fibers before and after the degradation test. Fully dried samples were coated with $\approx$1.3 nm platinum to ensure electrical conductivity. The alignment in all the cases follows a Gaussian distribution by using Equation (4), described in Figure S12, Supporting Information.

$$y = y_0 + \frac{A}{w\sqrt{\pi/2}} e^{-2\frac{(x-x_c)^2}{w^2}} \qquad (4)$$

Cytotoxicity Test: M-MSV-BALB/3T3 fibroblasts and C2C12 mouse myoblast cells were used to test the cytotoxicity based on ISO Standard 10993-5. Cells were cultured in a growth medium containing DMEM supplemented with 10% FBS Gold Plus, 1% GlutaMAX, 0.1% Gentamycin.

Cells were plated and grown to subconfluency prior to initiating the assays. Cells cultured without any contact with material were used as a blank control (Blank). For all assays, HDPE and ZDEC polyurethane were used as a negative (nontoxic) and positive (toxic) controls, respectively. Following the standard procedure, two indirect culturing methods (agar test and extract) were applied to evaluate whether there was a cytotoxic response to polymers. Samples were sterilized using 20 min UV under a steril bench.

For the agar test, after subconfluency of 75 000 cells/mL fibroblasts or 55 000 cells/mL myoblasts, a layer of autoclaved agarose gel with 37 °C (0.5% in DMEM) containing all supplements was cast on the top of the cell monolayer, and after 1 h of gelation, the sterilized fibrous scaffold (0.5 × 0.5 cm), as well as a same size piece of the positive and negative controls, were laid down on the gel. The materials and cells were incubated at 37 °C and 5% CO_2 for 24 h, after which the morphology changes of the cells were imaged using optical microscopy Leica DMi8 (Leica Microsystems, Germany).

Similarly, for the extract test, both cell lines were plated and grown to subconfluency 24 h before initiating the assay. The sterilized fibrous scaffold, as well as positive and negative controls, was incubated at 37 °C and 5% CO_2 with the 400 µL culture media for 24 h. After 24 h, the cell culture media was replaced with 350 µL of extract media. Cells were then incubated at 37 °C and 5% CO_2 for 24 h prior to cytotoxic evaluation. For the extract test, cytotoxicity of the material was evaluated qualitatively using fluorescence microscopy Leica DMi8 (Leica Microsystems, Germany) and quantitatively through the CellTiter-Blue Cell Viability Assay (Promega) and live/dead assay. The detail of these assays is presented in the Supporting Information.

Cell Culture: C2C12 mouse myoblast cells (with passage number less than 7) were cultured on aligned fibers made of the copolymer with a size of 4.0 cm^2. Before cell seeding, fibrous scaffolds were fixed in crowns (Scaffdex CellCrown inserts) with an effective internal area of 0.2 cm^2 and sterilized by washing them with ethanol 70% v/v for 30 min and exposing to UV light for 1 h under the clean bench. To enhance the cell adhesion on fibers, the scaffolds were coated with sterilized FNC solution for 1 h. Fibers without coating were tested as a control. Following the coating, a cell suspension with a density of 10^6 cell mL^{-1} was seeded on top to achieve a cell density of 150.000 cells cm^{-2} and incubated for 1 h to achieve the initial attachment of the cells. The growth medium for C2C12 cells containing DMEM, FBS serum 10% v/v, Pen/Strep 1%, Glutamin 4.0 mm, and HEPES 20.0 mm was added to the samples and was refreshed every 2nd day.

Live/Dead Assay, Proliferation Rate, and Alignment: The cell viability was analyzed using a live/dead assay and following the manufacturer protocol at different time points: 1, 3, and 7 days after the culture in the growth medium. A staining solution containing green fluorescent calcein AM in DPBS to target the esterase activity within the cytoplasm of living cells and the red fluorescence Ethidium homodimer-1 (EthD-1) was used to indicate dead cells. The samples were covered with the staining solution and incubated for 30 min at room temperature before imaging. After each time point, samples were visualized under the Nikon Eclipse Ti2 fluorescence microscope attached to a DS-Qi2 digital Nikon camera and Nis-D Elements v4.550 software was used for image analysis. The viability of the cells was calculated by counting the number of live and dead cells in ten different images from three different samples.

The proliferation rate of the myoblasts cells cultured on the fibers was measured using Alamar Blue assay after 1, 3, and 7 days of culture. According to the manufacturer´s protocol, 10% of reagent was added to the samples with the medium at each time point and incubated at 37 °C for 90 min and stirring gently every 30 min to avoid gradients. The reacted media from each sample was removed and kept on ice in the dark; 100 µL of that was transferred to a 96 well-plate, then its absorbance was measured using a plate reader (Berthold Tech TriStar2S, Germany) at 535 nm of excitation and 590 nm of emission wavelength. The negative control was prepared by mixing 10% Alamar blue in medium, and the positive control was prepared by mixing 10% reduced Alamar Blue in sterile MilliQ water. Three repeats were considered for each composition.

To quantify the alignment of the muscle cells on the fibers after 1, 3, and 7 days in culture, the actin filaments and nuclei were stained using a staining solution of Phalloidin DyLight 488 and DAPI in PBS to target rich regions in adenine and thymine in DNA and to label F-actin in fixed cells, respectively. First, the cell-cultured samples were fixed with formaldehyde (3.7%) solution for 15 min at room temperature. After washing with PBS, the cells were permeabilized with Triton (0.1%) solution for 5 min and washed with PBS. Next, the samples were covered and incubated with staining solution for 30 min at room temperature, followed by imaging using a fluorescence microscope. To determine cell alignment, morphological changes of nuclei were analyzed using ImageJ and orientation J plug-in in ten images from three different samples per day in culture. Nuclei orientation angles $-10° > x < 10°$ with respect to the fibers were considered as aligned.

Statistical Analyses: All results were treated using the software origin version 9.7 and were presented as mean ± standard deviation. All the values were averaged at least in triplicate, and statistical analyses were performed using a Student´s *t*-test and one-way analysis of variance. Tukey´s test was used to evaluate specific differences in values. A value of $p < 0.05$ was considered significant.

Supporting Information

Supporting Information is available from the Wiley Online Library or from the author.

Conflict of Interest

The authors declare no conflict of interest.

Data Availability Statement

The data that support the findings of this study are available in the supplementary material of this article.

[1] M. Ochi, N. Adachi, H. Nobuto, S. Yanada, Y. Ito, M. Agung, *Artif. Organs* **2004**, *28*, 28.

ADVANCED SCIENCE NEWS

www.advancedsciencenews.com

Macro-
molecular
Bioscience

www.mbs-journal.de

[2] C. Dieckmann, R. Renner, L. Milkova, J. C. Simon, *Exp. Dermatol.* **2010**, *19*, 697.

[3] H.-H. Sun, T. Jin, Q. Yu, F.-M. Chen, *J. Tissue Eng. Regener. Med.* **2011**, *5*, e1.

[4] J. Barthes, H. Özçelik, M. Hindié, A. Ndreu-Halili, A. Hasan, N. E. Vrana, *BioMed. Res. Int.* **2014**, *2014*, 18.

[5] S. Khalil, J. Nam, W. Sun, *Rapid Prototyping J.* **2005**, *11*, 9.

[6] A. D. Theocharis, S. S. Skandalis, C. Gialeli, N. K. Karamanos, *Adv. Drug Delivery Rev.* **2016**, *97*, 4.

[7] E. Gentleman, A. N. Lay, D. A. Dickerson, E. A. Nauman, G. A. Livesay, K. C. Dee, *Biomaterials* **2003**, *24*, 3805.

[8] B. B. Aaron, J. M. Gosline, *Biopolymers* **1981**, *20*, 1247.

[9] H. S. Rapoport, J. Fish, J. Basu, J. Campbell, C. Genheimer, R. Payne, D. Jain, *Tissue Eng., Part C* **2012**, *18*, 567.

[10] S. Miao, H. Cui, M. Nowicki, S.-J. Lee, J. Almeida, X. Zhou, W. Zhu, X. Yao, F. Masood, M. W. Plesniak, M. Mohiuddin, L. G. Zhang, *Biofabrication* **2018**, *10*, 035007.

[11] M. L. Muerza-Cascante, D. Haylock, D. W. Hutmacher, P. D. Dalton, *Tissue Eng., Part B* **2015**, *21*, 187.

[12] N. T. Saidy, F. Wolf, O. Bas, H. Keijdener, D. W. Hutmacher, P. Mela, E. M. De-Juan-Pardo, *Small* **2019**, *15*, 1900873.

[13] S. Agarwal, J. H. Wendorff, A. Greiner, *Adv. Mater.* **2009**, *21*, 3343.

[14] J. Uribe-Gomez, A. Posada-Murcia, A. Shukla, H. Alkhamis, S. Salehi, L. Ionov, *ACS Appl. Bio Mater.* **2021**, *4*, 5585.

[15] J. He, B. Zhang, Z. Li, M. Mao, J. Li, K. Han, D. Li, *Biofabrication* **2020**, *12*, 042002.

[16] J. Ding, J. Zhang, J. Li, D. Li, C. Xiao, H. Xiao, H. Yang, X. Zhuang, X. Chen, *Prog. Polym. Sci.* **2019**, *90*, 1.

[17] P. Katta, M. Alessandro, R. D. Ramsier, G. G. Chase, *Nano Lett.* **2004**, *4*, 2215.

[18] P. D. Dalton, D. Klee, M. Möller, *Polymer* **2005**, *46*, 611.

[19] I. Apsite, J. M. Uribe, A. F. Posada, S. Rosenfeldt, S. Salehi, L. Ionov, *Biofabrication* **2019**, *12*, 015016.

[20] J. Groll, T. Boland, T. Blunk, J. A. Burdick, D.-W. Cho, P. D. Dalton, B. Derby, G. Forgacs, Q. Li, V. A. Mironov, L. Moroni, M. Nakamura, W. Shu, S. Takeuchi, G. Vozzi, T. B. F. Woodfield, T. Xu, J. J. Yoo, J. Malda, *Biofabrication* **2016**, *8*, 013001.

[21] P. D. Dalton, *Curr. Opin. Biomed. Eng.* **2017**, *2*, 49.

[22] T. M. Robinson, D. W. Hutmacher, P. D. Dalton, *Adv. Funct. Mater.* **2019**, *29*, 1904664.

[23] T. D. Brown, P. D. Dalton, D. W. Hutmacher, *Adv. Mater.* **2011**, *23*, 5651.

[24] F. M. Wunner, O. Bas, N. T. Saidy, P. D. Dalton, E. M. D.-J. Pardo, D. W. Hutmacher, *J. Visualized Exp.* **2017**, *130*, e56289.

[25] G. Constante, I. Apsite, H. Alkhamis, M. Dulle, M. Schwarzer, A. Caspari, A. Synytska, S. Salehi, L. Ionov, *ACS Appl. Mater. Interfaces* **2021**, *13*, 12767.

[26] J. Uribe-Gomez, A. Posada-Murcia, A. Shukla, M. Ergin, G. Constante, I. Apsite, D. Martin, M. Schwarzer, A. Caspari, A. Synytska, S. Salehi, L. Ionov, *ACS Appl. Bio Mater.* **2021**, *4*, 1720.

[27] A. Tokarev, D. Asheghali, I. M. Griffiths, O. Trotsenko, A. Gruzd, X. Lin, H. A. Stone, S. Minko, *Adv. Mater.* **2015**, *27*, 6526.

[28] S.-J. Lee, D. Asheghali, B. Blevins, R. Timsina, T. Esworthy, X. Zhou, H. Cui, S. Y. Hann, X. Qiu, A. Tokarev, S. Minko, L. G. Zhang, *ACS Appl. Mater. Interfaces* **2019**, *12*, 2067.

[29] D. Asheghali, S.-J. Lee, A. Furchner, A. Gruzd, S. Larson, A. Tokarev, S. Stake, X. Zhou, K. Hinrichs, L. G. Zhang, S. Minko, *Nanomedicine* **2020**, *24*, 102152.

[30] C. Mueller, M. Trujillo-Miranda, M. Maier, D. E. Heath, A. J. O'connor, S. Salehi, *Adv. Mater. Interfaces* **2021**, *8*, 2001167.

[31] R. J. Spontak, N. P. Patel, *Curr. Opin. Colloid Interface Sci.* **2000**, *5*, 333.

[32] J. Chen, R. Dong, J. Ge, B. Guo, P. X. Ma, *ACS Appl. Mater. Interfaces* **2015**, *7*, 28273.

[33] Y. Hong, J. Guan, K. L. Fujimoto, R. Hashizume, A. L. Pelinescu, W. R. Wagner, *Biomaterials* **2010**, *31*, 4249.

[34] E. Ergene, B. S. Yagci, S. Gokyer, A. Eyidogan, E. A. Aksoy, P. Y. Huri, *Biomed. Mater.* **2019**, *14*, 025014.

[35] P. Kasprzyk, E. Sadowska, J. Datta, *J. Polym. Environ.* **2019**, *27*, 2588.

[36] S. G. Kim, D. S. Lee, *Macromol. Res.* **2002**, *10*, 365.

[37] I. Yilgör, E. Yilgör, G. L. Wilkes, *Polymer* **2015**, *58*, A1.

[38] D. Schönfeld, F. Chalissery, F. Wenz, M. Specht, C. Eberl, T. Pretsch, *Molecules* **2021**, *26*, 522.

[39] T. Pretsch, I. Jakob, W. Müller, *Polym. Degrad. Stab.* **2009**, *94*, 61.

[40] T. Pretsch, W. W. Müller, *Polym. Degrad. Stab.* **2010**, *95*, 880.

[41] M. Bothe, T. Pretsch, *J. Mater. Chem. A* **2013**, *1*, 14491.

[42] N. Fritzsche, T. Pretsch, *Macromolecules* **2014**, *47*, 5952.

[43] M. Hao-Yang, *J. Mater. Chem. B* **2017**, *5*, 4137.

[44] P. K. Behera, P. Mondal, N. K. Singha, *Polym. Chem.* **2018**, *9*, 4205.

[45] N. Mirtschin, T. Pretsch, *Polymers* **2017**, *9*, 98.

[46] D. Chalissery, T. Pretsch, S. Staub, H. Andrä, *Polymers* **2019**, *11*, 1005.

[47] M. Rogulska, A. Kultys, S. Pikus, *J. Therm. Anal. Calorim.* **2017**, *127*, 2325.

[48] C. Q. Huang, S. Y. Luo, S. Y. Xu, J. B. Zhao, S. L. Jiang, W. T. Yang, *J. Appl. Polym. Sci.* **2010**, *115*, 1555.

[49] D. S. Huh, S. L. Cooper, *Polym. Eng. Sci.* **1971**, *11*, 369.

[50] D. J. Martin, G. F. Meijs, G. M. Renwick, S. J. Mccarthy, P. A. Gunatillake, *J. Appl. Polym. Sci.* **1996**, *62*, 1377.

[51] J. Gosline, M. Lillie, E. Carrington, P. Guerette, C. Ortlepp, K. Savage, *Philos. Trans. R. Soc., B* **2002**, *357*, 121.

[52] H. Tobushi, H. Hara, E. Yamada, S. Hayashi, *Smart Mater. Struct.* **1996**, *5*, 483.

[53] S. Mondal, H. J. Lian, *Iranian Pol. J.* **2006**, *15*, 135.

[54] A. Lindström, A.-C. Albertsson, M. Hakkarainen, *Polym. Degrad. Stab.* **2004**, *83*, 487.

[55] A. K. Blakney, F. I. Simonovsky, I. T. Suydam, B. D. Ratner, K. A. Woodrow, *ACS Biomater. Sci. Eng.* **2016**, *2*, 1595.

[56] R. Scaffaro, A. Maio, F. Sutera, E. Gulino, M. Morreale, *Polymers* **2019**, *11*, 651.

[57] Y. Fu, G. Wu, X. Bian, J. Zeng, Y. Weng, *Molecules* **2020**, *25*, 3946.

[58] R. Al-Itry, K. Lamnawar, A. Maazouz, *Polym. Degrad. Stab.* **2012**, *97*, 1898.

2100427 (12 of 12)